ELSEVIER

Aerosol Science 35 (2004) 1189–1204

Journal of
Aerosol Science

www.elsevier.com/locate/jaerosci

Microparticle detachment from surfaces exposed to turbulent air flow: microparticle motion after detachment

A.H. Ibrahim, R.M. Brach, P.F. Dunn*

Particle Dynamics Laboratory, Department of Aerospace and Mechanical Engineering, University of Notre Dame, Notre Dame, IN 46556, USA

Received 7 January 2004; received in revised form 7 May 2004; accepted 17 May 2004

Abstract

The motion of heavy microspheres after their detachment from flat surfaces is considered. The microspheres initially are in static contact equilibrium, embedded fully in the viscous sublayer and subjected to a slowly accelerating fully developed turbulent flow. The equations of motion of the microspheres are presented, including surface roughness effects. The equations are solved numerically for detachment with and without consideration of a burst–sweep event initiating detachment. The microsphere velocity along the surface after detachment is measured using a strobed laser-light sheet and compared to the numerical solutions. Results indicate that the microspheres undergo pure rolling along the surface before possible entrainment and that the sweep plays a role in the detachment process. A model for predicting the microsphere velocity along the surface after detachment is presented.

Keywords: Microsphere; Detachment; Rolling; Turbulent flow

1. Introduction

The detachment of heavy microparticles due to air flow in the presence of surface contact adhesion is involved in many applications. This work is a further study made by the authors on the subject of microsphere detachment from surfaces. The authors presented experiments and a model for the free-stream flow velocity at which 50% of the microspheres detach by the fluid flow, U_{th}, under controlled experimental conditions (Ibrahim, Dunn, & Brach, 2003). This work presents measurements and a model for the microsphere velocity *after* detachment.

* Corresponding author. Tel.: +1-5746316089; fax: +1-5746318355.
E-mail address: pdunn@nd.edu (P.F. Dunn).

0021-8502/$ - see front matter © 2004 Elsevier Ltd. All rights reserved.
doi:10.1016/j.jaerosci.2004.05.003

Experimental observations show that particles detach from surfaces in discrete events, occurring at random intervals. This observation suggests that the detachment process has a statistical origin associated with the turbulent character of the flow. The concept of coherent structures has been used to describe the random nature of the turbulent flow near the surface and has been used in different resuspension models. Robinson (1991) reviewed the coherent structures in turbulent boundary layers. Cleaver and Yates (1973) developed a model for entrainment using the turbulent burst–sweep events. The bursts have been first observed by Kline, Reynolds, Schraub, and Runstadler (1967). The process begins with elongated counter-rotating stream-wise vortices that occur randomly in space and time. These subsequently cause near-wall fluid burst and sweep events (Corino & Brodkey, 1969). In the ejection part, $\dot{u} < 0$, $\dot{w} > 0$ and in the sweep part $\dot{u} > 0$, $\dot{w} < 0$, where $\dot{u}$ and $\dot{w}$ are the stream-wise and normal velocity fluctuations, respectively. However, Mollinger (1994) questioned whether these structures, that occur below $y^+ = yu^*/v$ of 10 (where y is the physical height above the surface, u^* is the friction velocity, and v is the dynamic viscosity of the fluid), affect microparticles immersed in the viscous sublayer. Alonso, Bolado, and Hontanon (1991) pointed out that some resuspension models assume that microparticles fully embedded within the viscous below y^+ of 5 do not resuspend. Yung, Merry, and Bott (1989) found that microparticles fully embedded in the viscous sublayer in *water* flow generally did not detach because of burst–sweep events, although some of them may detach.

Braaten, Shaw, and Paw (1993) identified two types of coherent structures associated with the entrainment of lycopodium microparticles 28 μm in diameter. The first pattern is called the ejection-sweep pattern, which is similar to the classical description of burst–sweep events and the second pattern is called the macro-sweep pattern. The latter was observed less frequently than the former and was characterized by a sustained high velocity periods with large sweeps.

The present work investigates the causality between microparticle detachment and burst–sweep events by measuring and modeling the microparticle velocities after detachment. In this work, stainless-steel micro-spheres were deposited onto a glass substrate under controlled conditions. The microspheres resided completely within the viscous sublayer and were initially in a state of contact equilibrium with adhesion and Hertzian forces.

The objectives of the current work are to validate a model of the motion of the microspheres after their detachment by a slowly accelerating fully developed turbulent flow and to investigate the causality between the burst–sweep event and the detachment. Numerical results are obtained for detachment with and without considering a burst–sweep event at the moment of detachment. The results then are compared to the measurements made using a strobed laser-light sheet.

Section 2 describes the experimental facility and techniques. The experimental results with their uncertainties are presented in Section 3. Section 4 presents the model and the numerical simulation of the microsphere velocities after detachment and compares the predicted results to the measurements. The conclusions of the work are summarized in Section 5.

2. Description of experiments

Ibrahim et al. (2003) provide a full description of the wind tunnel and the test section used in this study.

Stainless-steel microspheres (diameter: 64–76 μm; density: 8000 kg/m^3; Poisson's ratio: 0.28; Young's modulus: 215 GPa), were deposited unto a glass substrate (10 cm × 10.5 cm × 1.27 mm).

Deposition was made by gravitational settling from a height of about 5 cm to ensure non-plastic deformation upon contact. The deposition was made at a low deposition density (about 0.5 microspheres/mm^2) to produce a sparse monolayer, thereby minimizing collisions following detachment. Ibrahim, Dunn, and Brach (2004) found that the collisions between the microspheres can be neglected at this low number density. Most of the microspheres ($> 90\%$) were deposited as singlets and were not positioned in front of each other in the streamwise direction. The microspheres were embedded fully in the viscous sublayer of a fully developed turbulent flow. The density of the microspheres used was high enough (8000 kg/m^3) such that the microspheres, within the field of view, moved along the surface after detachment rather then lifting-off. The planar motion of the microspheres was an objective in itself, in order to eliminate all experimental and theoretical uncertainties associated with three-dimensional motion. This allowed better understanding of the flow mechanisms causing the detachment.

Similar glass substrates were used during experiments. One of the substrates was scanned by an atomic force microscope (AFM) under dry conditions. The mean of the standard deviations of its asperity heights was 17 Å. The histogram of the asperity heights is shown in Ibrahim et al. (2003). Caylor (1993) examined a sample of the stainless-steel microspheres using a scanning electron microscope and found that their surface was smooth to within the resolution of the instrument.

The progress of the free-stream velocity versus time was controlled through the programmable controller of the wind tunnel. The mean flow velocity was increased from zero up to one of a set of prescribed final free-stream velocities, U_∞ of either 5.74, 7.09 or 8.22 m/s at a mean flow acceleration of 0.014 m/s^2. The transient velocity profile can be fitted with a linear fit at an R^2 value of 99.4%. Ibrahim et al. (2003) found that the detachment process does not depend significantly upon the mean flow acceleration in the range 0.014–0.34 m/s^2. The air relative humidity was 52%.

A distributed roughness element was used at the inlet section to trigger the boundary layer to turbulence. The microspheres were deposited at a downstream distance of 1.4 m from the roughness element. Boundary layer velocity profiles were scanned at different velocities with a hot-wire probe. Good agreement was found with the data of Klebanoff (1955). In addition, the friction velocity, u^*, was statically calibrated against the free-stream velocity, as described in Ibrahim et al. (2003) and matched the empirical formulae for fully developed turbulent flow (e.g., Schlichting, 1979). The free-stream and friction velocities (in units of m/s) are correlated through a least-squares linear regression by the equation

$$u^* = 0.0375 U_\infty + 0.0387, \tag{1}$$

where the uncertainty is ± 0.0300 at a 95% confidence level.

The test section was illuminated with a strobed laser-light sheet. The schematic of the laser-light sheet technique is shown in Fig. 1. The laser beam was generated from a 3 W Argon-ion laser. The beam then passed through a disc of 3.7 cm radius that had 10 equidistant slots of 11 mm length each and that rotated at 2330 rpm. It then entered a fiber-optics cable and a plano-convex lens to generate a laser-light sheet on the test area on the substrate. A plano-convex lens was used to adjust the width and thickness of the sheet. When a microsphere detached, it left a trace on the image when the laser-light sheet was on and the trace disappears when the light was off. This mechanism allows the generation of alternating regions of brightness and darkness that last few milliseconds each.

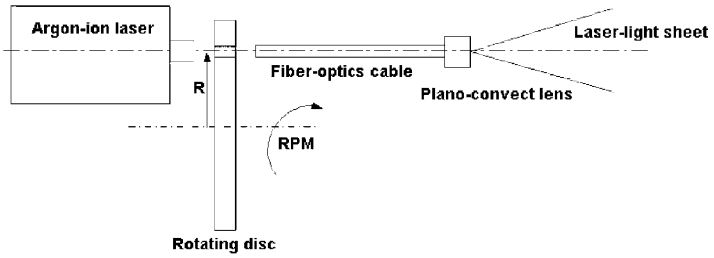

Fig. 1. Schematic of the strobed laser-light sheet used in the experiments.

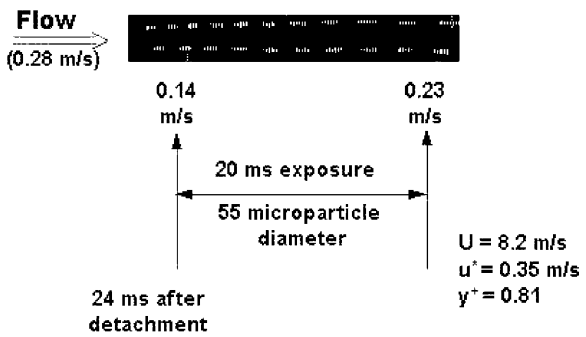

Fig. 2. Example picture of the laser traces obtained by the strobed laser-light sheet.

To avoid inaccuracy in measuring the trace length due to the closing of the camera shutter, no data were obtained from the first and last traces. To decrease the uncertainty in measuring the trace length, an average velocity was obtained over at least two of the middle traces and an optical magnification ratio of 21 was used to magnify the traces. This velocity was then corrected for averaging using polynomial curve fitting. No measurements were possible after the microspheres moved out of the field of view. This amounted to measuring the velocities in the first 70 ms at a U_∞ of 5.74 m/s and in the first 36 ms at a U_∞ of 8.22 m/s. An example picture of the microsphere traces is shown in Fig. 2.

3. Experimental results

The progress of the detachment fraction versus the free-stream velocity is presented in Fig. 3. This fraction is defined as

$$n^*(\tau) = 1 - \frac{n(\tau)}{n(0)}, \tag{2}$$

where $n(\tau)$ is the number of non-detached microspheres on the surface at time τ. The free-stream velocity at which $n^*(\tau)$ equals 0.5 is defined as the free-stream velocity for detachment, U_{th}. Ibrahim et al. (2003) found that the uncertainty in U_{th}, under controlled conditions, was in the range of $\pm$10–20%. The different symbols in Fig. 3 refer to different experiments made under the same

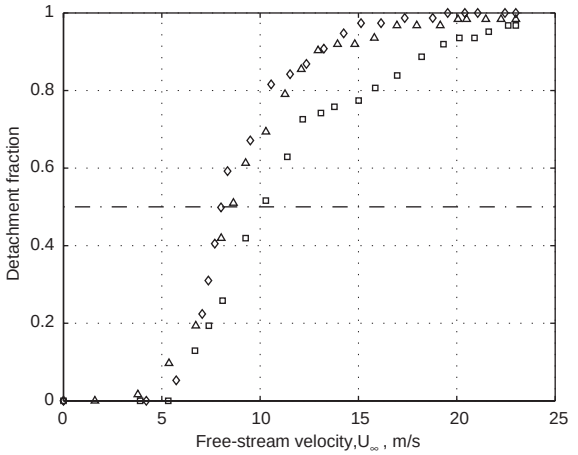

Fig. 3. Detachment fraction versus the free-stream velocity for stainless microspheres on glass. The relative humidity is 52% and the mean flow acceleration is 0.014 m/s^2. Different symbols refer to three experiments made under the same conditions.

conditions. The microvideographic observations of individual microspheres following detachment show that the particles move along the surface either by pure rolling, or rolling and sliding rather than by directly lifting-off the surface. The deviations from the main flow direction are within $\pm 20°$, as was shown in Ibrahim et al. (2003).

The motion of the particles on the surface after detachment was almost one-dimensional in the plane of the substrate and parallel to the flow direction. The measured microsphere velocities after detachment, v_p, versus time, τ, are shown in nondimensional form (v_{p1} versus τ_1) in Fig. 4, where

$$\tau_1 = \frac{\tau}{\tau_p}. \tag{3}$$

The microsphere relaxation time, τ_p, is defined as

$$\tau_p = \frac{2\rho_p R^2}{9\mu}, \tag{4}$$

where ρ_p and R are the microsphere density and diameter, respectively, and μ is the dynamic viscosity of air. The relaxation time characterizes the time required for a microsphere to adjust its velocity to a new condition of forces. It depends only on the microsphere and the medium and not on the nature or magnitude of the external forces. For a 70 μm diameter stainless-steel microsphere in air, the relaxation time is 119 ms. The nondimensional microsphere velocity, v_{p1}, is defined as

$$v_{p1} = \frac{v_p}{u_c}, \tag{5}$$

where u_c is the local flow velocity inside the viscous sublayer in the absence of any burst–sweep events at a height from the wall (surface) equal to the microsphere radius and is

$$u_c = \frac{Ru^{*2}}{v}, \tag{6}$$

where v is the kinematic viscosity of air.

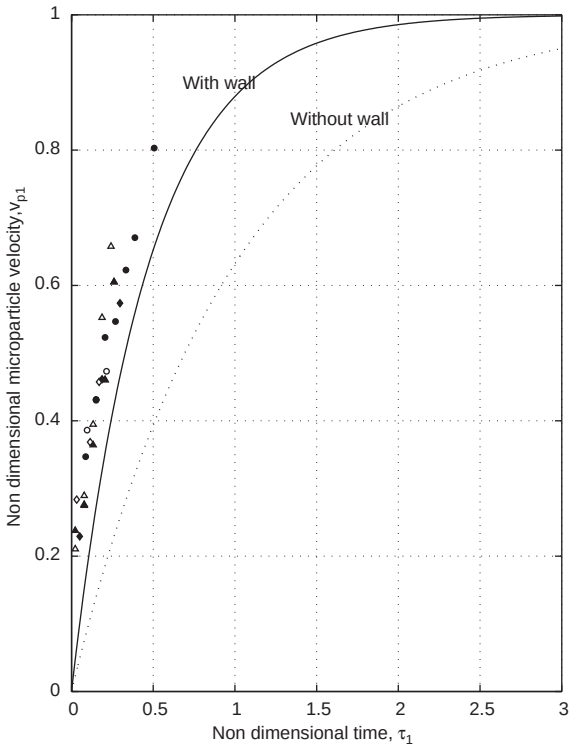

Fig. 4. Nondimensional measurements of the microsphere velocity along the surface after detachment. Solid curve: Simplified predictions with wall. Dotted curve: Without wall. The simplifications ignore the Basset and the inertial effects and the burst–sweep event. Symbols: Measurements at U_∞ (m/s) = 5.74 (○, ●), 7.09 (◇, ◆) and 8.22 (△, ▲).

It was observed that, in general, larger microspheres detach at lower free-stream velocities. At a relative humidity of 52%, the microspheres detached in the free-stream velocity range from 5 to 22 m/s. In order to account for the small diameter range used in this study, the microsphere diameter was estimated from the free-stream velocity at which it detached, as was shown in the model presented in Ibrahim et al. (2003).

The measured microsphere velocities are shown as symbols in Fig. 4 for different values of U_∞ ranging from 5.74 to 8.22 m/s. This corresponds to a microsphere Reynolds number $\tilde{R}e_p = Ru_c/v$ ranging from 0.39 to 0.69. Open and closed versions of the same symbol refer to *two* microspheres detaching at the same free-stream velocity and provide an indication of the combined effect of the experimental uncertainty and the different microsphere velocities at the same U_∞. Typical experimental uncertainties were 5% in velocity and 5% in time. The results show that the microspheres experience large accelerations over a short duration, causing them to acquire approximately 20% of u_c in only 2% of τ_p. This high acceleration does not continue. As the velocities increase, approximately 50% of τ_p is needed to reach 80% of u_c.

The data are compared with two simplified analytical models in Fig. 4: [1] microsphere motion in the absence of a wall (dotted curve), where the microsphere is given a step change in flow velocity from zero to a uniform u_c, [2] microsphere motion in the presence of the wall (solid curve), where

the microsphere is given a step change in velocity from zero to a linear velocity profile that has u_c at the microsphere center. These two do not include burst–sweep events, inertial correction to the Stokesian drag and the Basset effect (which is an effect that give rises to an additional drag force due to the unsteady nature of the flow, see for example, Crowe, Sommerfeld, & Tsuji, 1998). Section 4 includes these factors, discusses their effects and compares the predictions to the measured velocities. It is clear that the measured microsphere velocities consistently are greater than those for the two idealized cases.

4. Modeling

This section presents a model derived for estimating the motion of a microsphere fully embedded in viscous sublayer and subjected to a slowly accelerated fully developed turbulent flow after its detachment from the substrate. The motion is observed to be in the plane of the substrate and almost parallel to the main flow direction. In this model, $\tau = 0$ represents the time at which detachment is initiated by the flow. The equations of motion in the normal direction are analyzed in Section 4.1.1 and in the tangential direction in Section 4.1.2.

4.1. Equations of motion

The contact region of the microsphere and the surface is considered to be circular. Plastic deformation and dissipation are not considered. Also, it is assumed that contact is tangentially rigid and that the tangential deformation is neglected. Fig. 5 shows the local geometry, the coordinate system and the different forces and moments considered. The initial conditions correspond to static equilibrium and are as follows: At $\tau = 0$: $\theta = 0$, $\dot{\theta} = 0$, $t = 0$, $v_p = \dot{t} = 0$, $n = n_{eq}$, and $\dot{n} = 0$.

4.1.1. Equations of motions in the normal direction

Applying Newton's second law on the microsphere in the direction normal to the substrate

$$m\ddot{n} = F_H + F_A - mg + F_L(\tau), \tag{7}$$

where m is the microsphere mass and n is the normal coordinate of the mass center displacement. The first and second terms of the right-hand side of Eq. (7) are the Hertzian, F_H, and the adhesion forces, F_A, respectively. The third term, mg, is the gravity force and the last term is the aerodynamic lift force, $F_L(\tau)$. All these forces are normal to the surface.

The Hertzian force during contact, where $n \leqslant 0$, is

$$F_H = \sqrt{R}K(-n)^{3/2}. \tag{8}$$

The effective material stiffness, K, is

$$K = \frac{4}{3\pi(k_1 + k_2)}, \tag{9}$$

with

$$k_i = \frac{1 - \nu_i^2}{\pi E_i}, \tag{10}$$

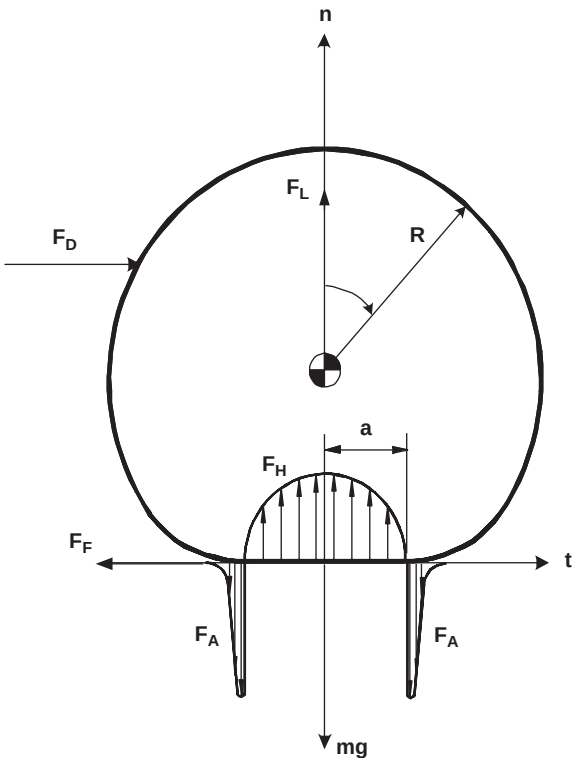

Fig. 5. Schematic of the microsphere on the surface with the forces and moments considered. F_H, F_A, F_D, F_L, F_F and mg are the Hertzian, adhesion, drag, lift, friction and gravity forces, respectively. n is the normal coordinate of the mass center displacement and t is the tangential coordinate.

where v_i and E_i are the Poisson's ratio and Young's modulus, respectively, for the sphere and the substrate materials.

The adhesion force is modeled as a ring force acting on the periphery of the circular contact area. This representation is not derived from basic principles but rather presents an idealization of the adhesion force as observed by others, such as Johnson, Kendall, and Roberts (1971), hereafter referred to as the JKR theory. This representation has been used in different studies by different investigators (see, for example, Brach & Dunn, 1995).

$$F_A = -2C\pi a f_0, \tag{11}$$

where a is the contact radius, which equals $\sqrt{-Rn}$ and is much smaller than the microsphere radius R. f_0 is the magnitude of the adhesion ring force over the circumference. Its value is set such that it generates the same equilibrium contact radius, a_{eq}, as the JKR theory. This condition yields (Li, Dunn, & Brach, 1999)

$$f_0 = \left(\frac{9KR\gamma^2}{2\pi}\right)^{1/3}, \tag{12}$$

where γ is the surface energy of adhesion.

The parameter C is the ratio of the rough pull-off force to the smooth pull-off force and accounts for the effects of surface roughness on adhesion. The effects of surface roughness on detachment have to be considered because real surfaces are rough. Roughness of the order of the atomic scale always is present, even for nominally "smooth" surfaces. Corn (1961) has observed that the resuspension is enhanced by roughness elements ranging from 0.22 to 0.48 μm on surfaces for particle diameters of several tens of micrometers. Kim, Rockfold, and Russell (1999) found that a surface roughness of only 45 Å is sufficient to reduce the normal pull-off force to a very small fraction of its smooth-surface value. Soltani (1993) shows for hard elastic materials that a surface roughness of the order of the atomic scale can reduce adhesion significantly. Cheng, Brach, and Dunn (2002) developed a model for the dependence of the factor C on the standard deviation of asperity heights. The value of C in this work is obtained through the model developed by Cheng et al. (2002), which relates the value of C to the standard deviation of asperity heights. According to this model, the measured standard deviation of asperity heights, 17 Å, corresponds to a value of C of approximately 1% in *dry* conditions (relative humidity $\lesssim$ 30%). The value of C increases with the relative humidity and is estimated in this work through the measured progress of the detachment fraction versus the free-stream velocity. Following Ibrahim et al. (2004), C is approximately 13% at a relative humidity of 52%.

The aerodynamic mean lift force, F_L, is obtained through the experimental results of Mollinger and Nieuwstadt (1996). They measured the mean and fluctuating lift forces on 120 and 218 μm diameter microspheres and obtained

$$F_L = (56.9 \pm 1.1)\rho v^2 R^{+(1.87\pm0.04)}, \tag{13}$$

where R^+ is defined as Ru^*/v and $0.3 < R^+ < 2$.

The mean lift and the gravity forces are *orders of magnitude less* than the Hertzian and adhesion forces. For example, the values of the Hertzian and adhesion forces are 0.1 and −0.1 mN, respectively, while the values of the gravity and the mean lift forces (at 8 m/s) are 14 and 10 nN, respectively. Given that the length scale of the surface roughness is much smaller than the microsphere contact radius and that the adhesion and Hertzian dissipation forces typically are smaller than the adhesion and Hertzian forces, the normal motion of the microsphere mass center is essentially governed by a balance of the Hertzian and adhesion forces. This implies that the mass center displacement, n, during and shortly following detachment remains approximately at its equilibrium value, n_{eq}, and that the mass center velocity, $\dot{n}$, is approximately zero at all times. Under these conditions, Eq. (7) reduces to

$$m\ddot{n} = F_H + F_A = 0. \tag{14}$$

At the time of detachment by a tangential force, the contact radius is equal to the equilibrium contact radius, a_{eq}, unlike the detachment by a lifting-off force, where it is equal to $4^{-1/3}a_{eq}$, according to the JKR theory.

4.1.2. Equations of motion in the tangential direction

Maxey and Riley (1983) and Maxey (1987) derived the equation of motion for an isolated particle in a nonuniform dynamic flow field including the gravity, buoyancy, pressure, virtual mass, Basset, Faxen and Stokesian drag forces. The pressure term is caused by the pressure gradient in the fluid surrounding the microsphere as the local fluid element accelerates.

The virtual, or added, mass force considers the force required to accelerate the surrounding fluid. The Basset, or history, force describes the force due to the lagging boundary layer development with the changing relative velocity and is associated with past movements of the microsphere. The Faxen force results from the nonuniformity of the flow field.

In this work, the buoyancy, pressure, and the virtual mass forces can be neglected compared to the drag force because the density of the microspheres used is approximately 6800 times that of the air.

The Faxen force also is neglected, based on the numerical results of Kurose and Komori (1999) of the effects of the fluid shear on a rotating rigid sphere in a homogeneous linear shear flow at low Reynolds numbers.

Hjemfelt and Mackros (1966) found that the Basset effect is insignificant if [1] the particle-to-fluid density ratio ρ_p/ρ_f is 10^3 or more *and* [2] $\sqrt{(\mu/\rho_f \omega D^2)} > 6$ where ω is the frequency of the flow oscillation. In this work, although the microsphere-to fluid density is large enough, this effect may be important due to the large microsphere acceleration observed at low τ_1. This effect will be considered using the results of Sano (1981). Sano developed a correction factor to account for the Basset and inertial effects for a microsphere undergoing an impulsively started motion at $\tilde{R}e_p = (u_c R)/\nu \ll 1$.

The drag force arises from the difference between the local flow velocity, u_c and the microsphere velocity, $v_p(\tau)$, and is the driving force for detachment and for the microsphere motion after detachment. The motion of the microsphere is assumed to be parallel to the plane of the substrate and in the mean flow direction. These assumptions are justified by the experimental observations.

Applying Newton's second law on the microsphere in the tangential direction, t, and following the representation shown in Fig. 5

$$F_D - F_F = m\dot{v}_p, \tag{15}$$

and

$$M_D + F_F R = 0.4mR^2\ddot{\theta}, \tag{16}$$

where F_D is the aerodynamic drag force, corrected for the Basset, inertial, and wall effects. M_D is the aerodynamic drag moment, F_F is the frictional force, t is the tangential coordinate of the mass center displacement of the sphere, and θ is the rotational coordinate. M_D is given by (O'Neill, 1968)

$$M_D = 7.551944\pi\mu(u_c - v_p)R^2. \tag{17}$$

The motion is considered to be pure rolling ($v_p - R\dot{\theta} = 0$) if the obtained friction force from Eqs. (15) and (16) is less than $\mu_f F_H$. Slipping occurs ($F_F = \mu_f F_H$) if the obtained friction force is equal to or larger than $\mu_f F_H$. The dynamic friction coefficient, μ_f, is assumed to be 0.16 (Brach, Dunn, & Li, 2000). It should be noted that the friction force is not zero in the pure rolling case as long as $\dot{v}_p$ is not zero.

The numerical results show that the motion after detachment corresponds to pure rolling. Consequently, Eqs. (15) and (16) can be re-written as

$$\dot{v}_p = \frac{(1.74)RF_D}{1.4mR}, \tag{18}$$

and

$$\ddot{\theta} = \frac{\dot{v}_p}{R}. \tag{19}$$

4.1.3. Modeling the drag force

The microsphere Reynolds number, $Re_p = (u_c - v_p)R/\nu$, is less than one for the velocity range considered. The drag force is modeled as Stokesian drag, $D_s = 6\pi\mu R(u - v_p)$ with two corrections. First, the Stokesian drag is multiplied by a factor ψ ($\psi > 1$), which accounts for the combined inertial and Basset effects (Sano, 1981). Second, the drag force is corrected for the presence of the wall using the results of O'Neill (1968). These two corrections are assumed to be additive because of the linearity of the governing equations at the low Reynolds number limit. The maximum $\tilde{R}e_p(u_cR/\nu)$ considered is 0.69. The drag force therefore is modeled as

$$F_D(\tau) = 1.7009\psi D_s, \tag{20}$$

where the factor ψ is given by

$$\psi = H(\tau_2) + \frac{\delta(\tau_2)}{3} + (\pi\tau_2)^{-1/2} + \frac{3}{8}\tilde{R}e\left[\left(1 + \frac{4}{\tilde{R}e^4\tau_2^2}\right)\operatorname{erf}\left(\frac{\tilde{R}e\sqrt{(\tau_2)}}{2}\right) + \left(\frac{2}{(\pi\tau_2)^{1/2}\tilde{R}e}\right)\right.$$
$$\left.\times\left(1 - \frac{2}{\tilde{R}e^2\tau_2}\right)\exp\left(-\frac{\tilde{R}e^2\tau_2}{4}\right) - \left(\frac{8}{3(\pi\tau_2)^{1/2}\tilde{R}e}\right)\right] + \left[\frac{9\tilde{R}e^2\ln\tilde{R}e}{40}\right] + [0.1879\tilde{R}e^2]. \tag{21}$$

τ_2 is a second time scale defined as

$$\tau_2 = \frac{\tau\nu}{R^2}, \tag{22}$$

and $H(\tau_2)$ and $\delta(\tau_2)$ denote the heavy-side and the Dirac delta functions, respectively. The two time scales τ_1 and τ_2 are related by $\tau_1 = (\tau_2R^2)/(\tau_p\nu)$. At times $\tau_2 \ll 1/\tilde{R}e^2$, Eq. (21) can be written as

$$\psi = H(\tau_2) + \frac{\delta(\tau_2)}{3} + (\pi\tau_2)^{-1/2} + O(\tilde{R}e^2). \tag{23}$$

Eq. (23) has an integrable singularity of order $-\frac{1}{2}$ at zero time. The solution is started at a time $\tau_2 = \varepsilon = 0.001\tilde{R}e^2$. Using Eqs. (18), (20), and (23), the microsphere velocity $v_p|_\varepsilon$ is obtained as $u_c(1 - \exp[-5.5928\mu(\varepsilon + \frac{1}{3} + 2\sqrt{(\varepsilon/\pi)})/\rho_p])$. The numerical solution at larger times is obtained by integrating Equations (18), (20), and (21) with initial conditions $\tau_2 = \varepsilon$ and $v_p = v_p|_\varepsilon$. For small values of ε, the solution is independent of the value of ε.

The factor ψ accounts for the combined Basset and inertial effects. In the absence of these two effects, ψ is 1. The Basset effect is apparent at low time, and diminishes after τ_1 of approximately 0.1. For example, for the microsphere detaching at U_∞ of 5.74 m/s, $\psi = 5$ at $\tau_1 = 3.5\times10^{-5}$ ($\tau_2 = 0.0529$) but quickly decreases to 1.17 at $\tau_1 = 0.1$ ($\tau_2 = 151$). This behavior is shown in Fig. 6. Fig. 7 shows the predicted microsphere velocity with and without considering the combined inertial and Basset effects at $U_\infty = 5.74$ m/s in the *absence* of a burst–sweep event. The measured data points suggest that the relatively high value of ψ at low τ_1 is only *partially* responsible for the high microsphere acceleration at low τ_1.

The effect of the burst–sweep event on the drag force is accounted for through the measurements of Thomas and Bull (1983). They measured the profile of the burst–sweep event at $y^+ = 30$. In the burst part of the event, $\acute{u} < 0$, $\acute{w} > 0$ and in the sweep part $\acute{u} > 0$, $\acute{w} < 0$, where $\acute{u}$ and $\acute{w}$ are the streamwise and normal velocity fluctuations, respectively, and u is the mean streamwise flow velocity. The time scale of the measured profile is $\tau_3 = (\tau U_\infty)/\delta^*$, where δ^* is the boundary layer displacement thickness ($\tau_1 = \tau_3\delta^*/(\tau_pU_\infty)$).

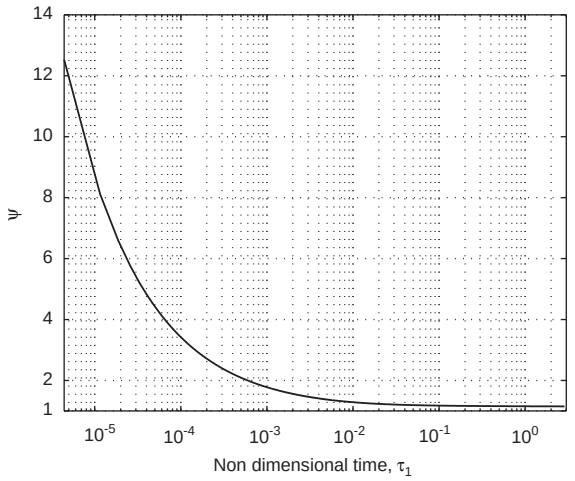

Fig. 6. Variation of the factor ψ with time. Based on the results of Sano (1981) $U_\infty = 5.74$ m/s and $\tilde{Re}_p = 0.39$.

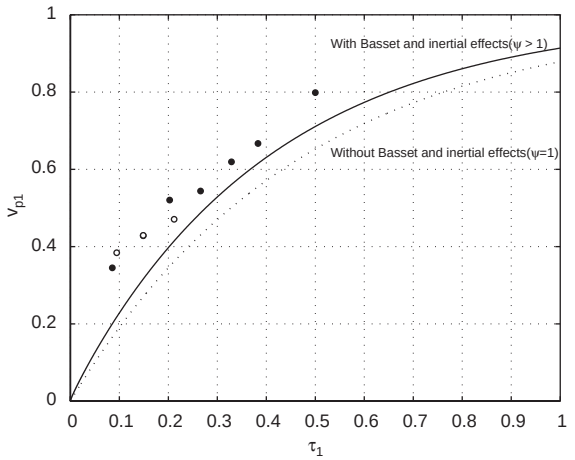

Fig. 7. Microsphere velocities after detachment with considering the Basset and the inertial effects (solid curve) and without considering these effects (dotted curve). Same flow conditions as in Figure 6.

In this profile, during the burst part, the fluctuating mean-stream velocity, $\acute{u}$, is zero at $\tau_3 = 0$, then it decelerates non-linearly up to a minimum of $0.33u$ at $\tau_3 = 24.5$ before it returns to zero at $\tau_3 = 25.4$. In the sweep part, it accelerates from zero up to a maximum of $1.43u$ at $\tau_3 = 26.6$ before it returns to zero at $\tau_3 = 43$.

Soltani and Ahmadi (1995) performed a direct numerical simulation of microsphere entrainment in a turbulent channel flow. Their results show that the peak instantaneous streamwise velocity during the burst–sweep event can be expressed as

$$u^+ = \Phi y^+, \tag{24}$$

where the mean of Φ is 1.84 and the minimum and maximum values of Φ are 1.6 and 2.14, respectively.

A simplified solution can be obtained by setting $\psi = 1$ and assuming that burst–sweep events do not play a role in the detachment process. For this case, Eqs. (18), (20), and (21) reduce to

$$\dot{v}_p = \frac{12.68\pi\mu R(u_c - v_p)}{m} \tag{25}$$

and

$$\ddot{\theta} = \frac{\dot{v}_p}{R}. \tag{26}$$

Integrating Equation (25) subject to the initial condition $v_p = 0$ at $\tau = 0$, and nondimensionalizing yields to

$$v_{p1}(\tau_1) = 1 - \exp\left(-\frac{\tau_1}{0.47}\right). \tag{27}$$

Eq. (27) is plotted as a solid curve in Fig. 4. The dotted curve in the same figure is for the case of $v_{p1}(\tau_1) = 1 - \exp(-\tau_1)$, which corresponds to a microsphere given a step change in velocity from zero to a uniform u_c in the absence of the wall and neglecting inertial and Basset effects. These two cases represent first-order systems of time constants $0.47\tau_p$ and τ_p, respectively, where the motion is pure rolling in the first case. The lower time constant in the first case is caused by the increase in the drag force due to the presence of the wall and to the negative friction force in Fig. 5. The friction force opposes the relative motion at the point of the contact. In case of pure rolling, the point of contact moves in the direction opposite to the drag force.

Now, considering the Basset and inertial effects ($\psi > 1$), and the burst–sweep events, Eqs. (18), (20), and (21) can be integrated numerically using Runge–Kutta integration and a variable time-step. Solution are presented in Fig. 8 for a microsphere detaching at different values of U_∞ for detachment without burst–sweep events (dotted curve) and detachment starting at the start of the sweep pattern in the burst–sweep event (solid curve).

Fig. 8 shows reasonable agreement between the measurements and the model. It also reveals that the microsphere velocities are higher than those predicted when neglecting the causality between burst–sweep events and detachment, suggesting that detachment is related to these or similar events. Moreover, the results suggest that the detachment more likely is related to a structure having an instantaneous mean stream velocity *higher* than the mean. This suggests that detachment is related to the sweep part of the structure rather than to the burst part. This is in accordance to the experimental observations that the incipient motion is along the surface rather than lift-up normal to the surface. This is supported further by the fact that the effects of the ejection bursts diminishes when approaching the viscous sublayer so that only the sweep is observed (Hinze, 1975). Also, Brodkey, Wallace, and Eckelmann (1974), for experiments in fully developed open channel flow, observed that although ejection events originated wholly outside the viscous sublayer, sweep motions could travel all the way to the wall.

Fig. 8 also suggests that some microspheres detach with sweeps of different intensities (different values of Φ) and/or during various parts of the sweep profile. This implies that detachment does not necessarily take place at the start of the sweep pattern, but rather during any point during the sweep pattern.

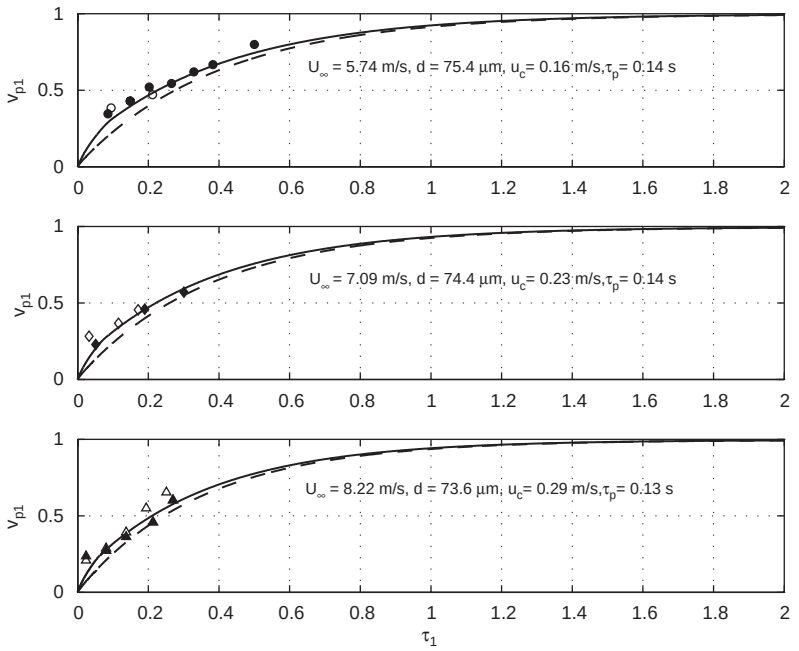

Fig. 8. Microsphere velocities after detachment with considering the sweep event (solid curve) and without considering this event (dotted curve).

Furthermore, it is was shown in Ibrahim et al. (2003), based on kinetics arguments, that the incipient motion at the time of detachment is pure rolling. This is because the moment and force balances predicted that the pure rolling resistance is much smaller than the sliding or lift-off resistances. In this work, the numerical simulation shown in Figs. 4 and 8 had the resultant friction force, F_F, less than the sliding friction force, $\mu_f F_H$. This indicates that pure rolling is taking place during subsequent motion for all practical values of μ_f before possible entrainment. Hence, the rotation rate $\dot{\theta}$ equals v_p/R. Fig. 9 shows the numerical solutions of the microsphere velocity, rotation rate, drag and friction forces forces for a microsphere detaching at a U_∞ of 5.74 m/s.

5. Summary and conclusions

This work considers microspheres fully embedded in the viscous sublayer of a fully developed turbulent flow. The equations of motion in the normal and tangential directions are presented, analyzed, numerically solved, and compared to the measurements. The equations consider the contact forces, the effects of the surface roughness, the Basset effect and burst–sweep events. The results indicate that the normal direction is governed practically by a balance of the Hertzian and adhesion forces. In contrast with the entrainment case, the mass center displacement and the contact radius are approximately at their equilibrium position after detachment. In the tangential direction, the microspheres undergo pure rolling on the surface following detachment and a high acceleration up to τ_1 of approximately 0.02. Measurements suggest that this high acceleration is caused mainly by

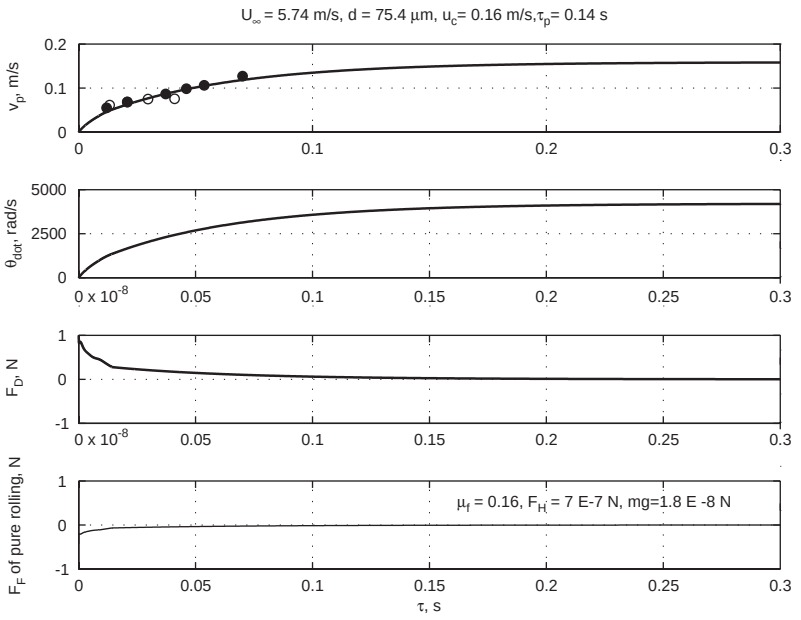

Fig. 9. Microsphere velocities after detachment with considering the sweep event (solid curve) and without considering this event (dotted curve). Same flow conditions as in Figure 6.

the sweep part of the burst–sweep event. The measurements also indicate that, at least shortly after detachment, the adhesion dissipation moment can be neglected compared to the drag moment.

Acknowledgements

Research described in this article was supported by Philip Morris USA, Incorporated.

References

Alonso, A., Bolado, R., & Hontanon, E. (1991). *Aerosol resuspension in the reactor cooling system of LWR's under severe accident conditions*. Final Report, Commission of the European Communities, EUR 13789 EN, 44.

Braaten, D. A., Shaw, R. H., & Paw, U. K. T. (1993). Boundary layer flow structures associated with particle reentrainment. *Boundary Layer Meteorology*, *65*, 255–272.

Brach, R. M., & Dunn, P. F. (1995). Macrodynamics of microparticles. *Aerosol Science and Technology*, *23*, 51–71.

Brach, R. M., Dunn, P. F., & Li, X. (2000). Experiments and engineering models of microparticle impact and deposition. *Journal of Adhesion*, *74*, 227–282.

Brodkey, R. S., Wallace, J. M., & Eckelmann, H. (1974). Some properties of truncated turbulence signals in bounded shear flows. *Journal of Fluid Mechanics*, *66*, 209–224.

Caylor, M. J. (1993). *The impact of electrically charged microspheres with planar surfaces under vacuum conditions*. Ph.D. Dissertation, University of Notre Dame.

Cheng, W., Brach, R. M., & Dunn, P. F. (2002). Surface roughness effects on microparticle adhesion. *Journal of Adhesion*, *78*, 929–965.

Corino, E. R., & Brodkey, R. S. (1969). Visual investigation of the wall region in turbulent flow. *Journal of Fluid Mechanics*, *37*, 1–30.

Corn, M. J. (1961). The adhesion of solid particles to solid surfaces II. *Journal of the Air Pollution Control Association*, *11*, 566–575.

Cleaver, J. W., & Yates, B. (1973). Mechanism of detachment of colloidal particles from a flat substrate in a turbulent flow. *Journal of Colloid and Interface Science*, *44*, 464–474.

Crowe, C., Sommerfeld, M., & Tsuji, Y. (1998). *Multiphase flows with droplets and bubbles*. New York: CRC Press.

Hjemfelt, A. T., & Mackros, L. F. (1966). Motion of discrete particles in a turbulent fluid. *Applied Scientific Research*, *16*, 149–161.

Hinze, J. O. (1975). *Turbulence*. New York: McGraw-Hill.

Ibrahim, A. H., Dunn, P. F., & Brach, R. M. (2003). Microparticle detachment from surfaces exposed to turbulent air flow: controlled experiments and modeling. *Journal of Aerosol Science*, *34*, 765–782.

Ibrahim, A. H., Dunn, P. F., & Brach, R. M. (2004). Microparticle detachment from surfaces exposed to turbulent air flow: Effects of flow and particle deposition characteristics. *Journal of Aerosol Science*, in press, doi: 10.1016/j.aerosci.2004.01.002.

Johnson, K. L., Kendall, K., & Roberts, A. D. (1971). Surface energy and the contact of elastic solids. *Proceedings of the Royal Society of London, Series A*, *324*, 301–313.

Kim, H., Rockfold, L., & Russell, T. (1999). Adhesion to rough surfaces. In *American physical society centennial meeting program*, Atlanta, Georgia.

Klebanoff, P. S. (1955). Characteristics of turbulence in a boundary layer with zero pressure gradient. *NACA technical report 1247* (http://naca.larc.nasa.gov/).

Kline, S. J., Reynolds, W. C., Schraub, F. A., & Runstadler, P. W. (1967). The structure of turbulent boundary layers. *Journal of Fluid Mechanics*, *30*, 741–773.

Kurose, R., & Komori, S. (1999). Drag and lift forces on a rotating sphere in a linear shear flow. *Journal of Fluid Mechanics*, *384*, 183–206.

Li, X., Dunn, P. F., & Brach, R. M. (1999). Experimental and numerical studies on the normal impact of microspheres with surfaces. *Journal of Aerosol Science*, *30*, 439–449.

Maxey, M. R. (1987). The motion of a small rigid sphere in a nonuniform flow. *Physics of Fluids*, *30*, 1579–1582.

Maxey, M. R., & Riley, J. J. (1983). Equation of motion for a small rigid sphere in a nonuniform flow. *Physics of Fluids*, *26*, 883–889.

Mollinger, A. M. (1994). *Particle entrainment—measurements of the fluctuating lift force*. Ph.D. Dissertation, Technical University of Delft, The Netherlands, p. 185.

Mollinger, A. M., & Nieuwstadt, F. T. M. (1996). Measurements of the lift force on a particle fixed to the wall in the viscous sublayer of a fully developed turbulent boundary layer. *Journal of Fluid Mechanics*, *316*, 285–306.

O'Neill, M. E. (1968). A sphere in contact with a plane wall in a slow linear shear flow. *Chemical Engineering Science*, *23*, 1293–1298.

Robinson, S. K. (1991). Coherent motions in the turbulent boundary layer. *Annual Review of Fluid Mechanics*, *23*, 601–639.

Sano, T. (1981). Unsteady flow past a sphere at low Reynolds number. *Journal of Fluid Mechanics*, *112*, 433–441.

Schlichting, H. (1979). *Boundary layer theory*. New York: McGraw-Hill.

Soltani, M. (1993). *Mechanisms of particle removal due to turbulent flow or substrate acceleration*. M.Sc. Thesis, Clarkson University.

Soltani, M., & Ahmadi, G. (1995). Direct numerical simulation of particle entrainment in turbulent channel flow. *Physics of Fluids*, *7*, 647–657.

Thomas, A. S. W., & Bull, M. K. (1983). On the role of wall pressure fluctuations in deterministic motions in the turbulent boundary layer. *Journal of Fluid Mechanics*, *128*, 283–322.

Yung, B. P. K., Merry, H., & Bott, T. R. (1989). The role of turbulent bursts in particle re-entrainment in aqueous systems. *Chemical Engineering Science*, *44*, 873–882.